Chapter 8

Transparent Conducting Oxides for Active Plasmonics

8.1 Introduction

In this chapter, a third method for mode modulation within MIM waveguides is discussed. Here we use transparent conducting oxides (TCOs) as the active layer within the waveguide. These materials can achieve carrier concentrations on the order of 1×10^{19} - 1×10^{21} cm^{-3}. Based on Drude model calculations, this results in plasma frequencies at near infrared and visible frequencies. By tuning the plasma frequency close to the frequency of operation of these devices, changes in the real part of the refractive index on the order of $\Delta \mathrm{n}_{index} = 1$ are achieved. Here we demonstrate switching in such a device with an MOS geometry. Structures were fabricated with gold as the top and bottom cladding layers and a layer of TCOs and silicon dioxide were sputter deposited between the metal layers. Spectroscopic ellipsometry was used to measure the complex indicies of refraction within the multi-layer stack and determine the extent to which the effective index of the supported optical modes was shifted. [1]

8.2 Carrier Modulation in Active Plasmonics

The field of active plasmonics is continually exploring new methods of plasmon mode modulation. Different waveguiding geometries have been developed that take advantage of optical switching in: thermally modulated systems [38], liquid crystal layers [41, 120], quantum dots [84], and ferroelectric films which was reported in the literature [31, 33, 70], as well as in Chapter 6.

In Chapter 7, modulation of the plasmon modes within a waveguide was demonstrated by modulating the carrier density within the dielectric layer of the MIM waveguide. This device had the benefit of being extremely fast (sub nano-second switching) as well as being CMOS compatible. However, the electro-optic effect in silicon is very small [107], and the change in index of refraction

---

[1]This chapter is based on work done with Dr. Eyal Feigenbaum.

for even highly doped silicon is also small. Based on the Drude-Lorentz model [98]:

$$\Delta n_{index} = \frac{-e^2 \lambda_0^2}{8\pi^2 c^2 \epsilon_0 n_{index}} \left(\frac{\Delta n}{m_e^*} + \frac{\Delta p}{m_h^*} \right) \tag{8.1}$$

forming an accumulation layer in an MOS device (with an accumulation layer of $\Delta n = 10^{19}$ cm^{-3}), $\Delta n_{index} \simeq 0.002$ at $\lambda = 800$ nm and $\Delta n_{index} \simeq 0.009$ at $\lambda = 1500$ nm. In Equation 8.1, m_e^* and m_h^* are the effective masses of the electrons and holes, respectively; and Δn and Δp are the changes in electron and hole concentrations (respectively) that induce a change in index of refraction, Δn_{index}. For the plasMOStor, the solution to this issue was to design the structure in such a way that there was exactly one photonic mode that was near cutoff. This produced large switching ratio's for a material with lower ($n = 9 \times 10^{16}$ cm^{-3}) carrier concentrations.

An alternative solution to this problem is to chose a dielectric material whose carrier density is much higher, and as a result, will have a plasma frequency closer to the visible and near infrared frequencies of interest. Based on the Drude model:

$$\epsilon = \epsilon_\infty - \frac{\omega_p^2}{\omega^2 + i\omega\omega_\tau} \tag{8.2}$$

Here, ϵ_∞ is the high frequency dielectric constant, ω_τ is the scattering frequency, and ω_p is the plasma frequency given by:

$$\omega_p = \frac{ne^2}{\epsilon m^*} \tag{8.3}$$

where m^* is the effective electron mass and n is the carrier concentration. The resulting change in ω_p as a function of carrier density is shown in Figure 8.1. In this figure, $\epsilon_\infty = 1$, $\omega_\tau = 0$, and $m^* = m_e$. The corresponding plasma frequency is given by the points where $\epsilon = 0$. As can be seen from the figure, by working with carrier concentrations on the order of $10^{20} - 10^{21}$ cm^{-3}, the plasma frequency of the layer will lie in the near infrared to visible frequency regime.

One family of materials that would satisfy these requirements is Transparent Conducting Oxides (TCOs). Both indium tin oxide (InTiO$_3$) and indium zinc oxide (InZnO$_3$) are degenerately doped oxides that are widely used as electrical contacts in solar cells, light emitting diodes, flat screen televisions, and cellular phone displays. These materials can be doped to have carrier concentrations between $10^{19} - 10^{21}$ cm^{-3} based on manipulating the number oxygen vacancies and interstitial metal dopants. At the same time, these TCOs can have greater than 80% transmittance at visible frequencies [111]. Instead of using these materials as transparent contacts, in this
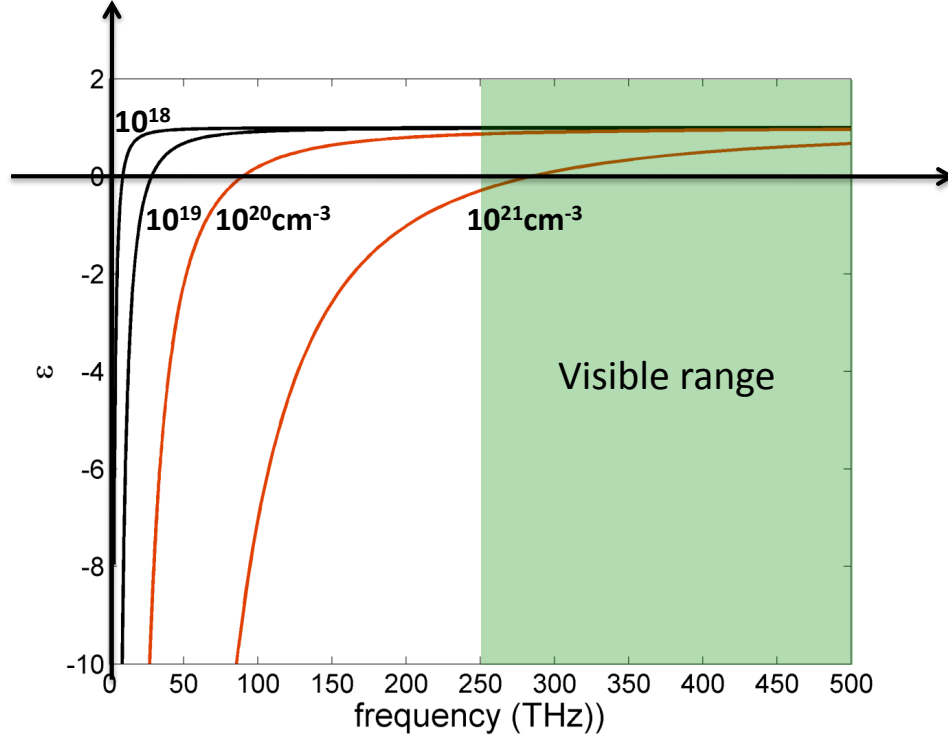
Figure 8.1. For this material: $\epsilon_\infty = 1$, $\omega_\tau = 0$, and $m^* = m_e$. The plasma frequency is given where $\epsilon = 0$.

chapter we demonstrate that these TCOs can be used as the <u>active semiconductor</u> within a MIM waveguide. These materials are used in a metal-oxide-semiconductor (MOS) structure similar to that of the plasmostor in Chapter 7 (Figure 8.2); and under an applied field, the device will form an accumulation layer. We show that by increasing the carrier concentration within the ~ 5 nm thick accumulation layer, the real part of the index of refraction can be shifted on the order of $\Delta \mathrm{n}_{index} = 1$.

8.3   Fabrication and Characterization

For all experiments, $InTiO_3$ and $InZnO_3$ films were deposited using RF magnetron sputtering in and oxygen/argon plasma. All depositions were done at room temperature and 3 mTorr pressure within the chamber. For TCO depositions, the gas during sputtering was 1.29% O_2 and 98.71% Ar, and the films were sputtered at 200 W. The targets used were $(In_2O_3)_{0.9}(ZnO)_{0.1}$, and $(In_2O_3)_{0.9}(TiO)_{0.1}$ weight percent. For silicon dioxide (SiO_2) depositions, the gas during sputtering was 28.45% O_2
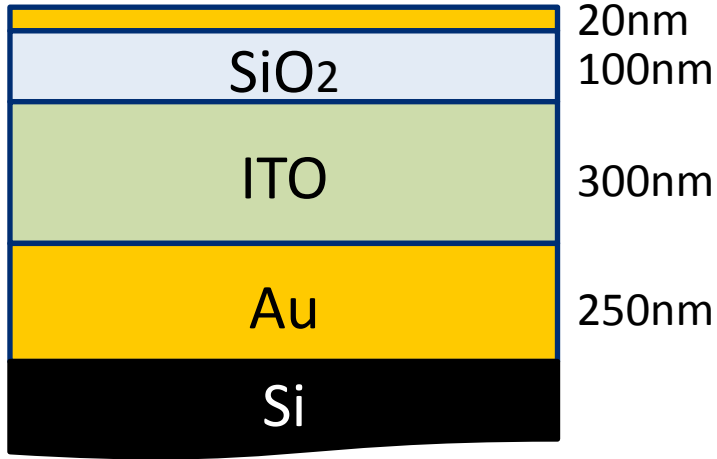
Figure 8.2. MOS structure used in the ellipsometry studies.

and 71.55% Ar, and the films were sputtered at 224 W. All gold films were deposited using thermal evaporation.

Films were characterized using Hall probe measurements and spectroscopic ellipsometry. The specifics of spectroscopic ellipsometry are covered in Appendix C. Films of $InTiO_3$ were deposited on quartz slides and Hall probe measurements determined that the electron mobility in these films was $\mu = 14.5$ cm$^2/Vs$ and the electron equilibrium concentration was n $= 5 \times 10^{20}$ cm^{-3}.

To characterize the films in ellipsometry: Au, SiO_2, and $InTiO_3$ layers were deposited independently onto silicon substrates. All layers were measured from $\lambda = 460$ - 820 nm. The layers were then deposited in a MOS structure shown in Figure 8.2. The layered structure deposited on silicon consisted of: 250 nm Au, 300 nm $InTiO_3$, 100 nm SiO_2, and a 20 nm semi-transparent top Au electrode. Fitting Ψ and Δ for each of the layers as well as the entire layer stack was done by minimizing the mean-square error between the model and measured data by varying the materials parameters. The SiO_2 films were modeled using a Cauchy layer (given by Equations D.1 and D.2) with $n_0 = 1.097, n_1 = 1405.8, n_2 = -1243.3, k_0 = 0.038, k_1 = -385.71, k_2 = 977.155, C_0 = 10^2, C_1 = 10^7$, and λ is given in nm. The $InTiO_3$ layer was modeled as a Drude layer with: $\lambda_p = 2300$ nm, $\tau = 1$ fs, and $\epsilon_\infty = 4.2$, and the value of λ_p was confirmed using Fourier transform infrared spectroscopy. As a result we obtained $n = 1 \times 10^{20}$ cm^{-3}, which is in good agreement with the value measured from the Hall probe.

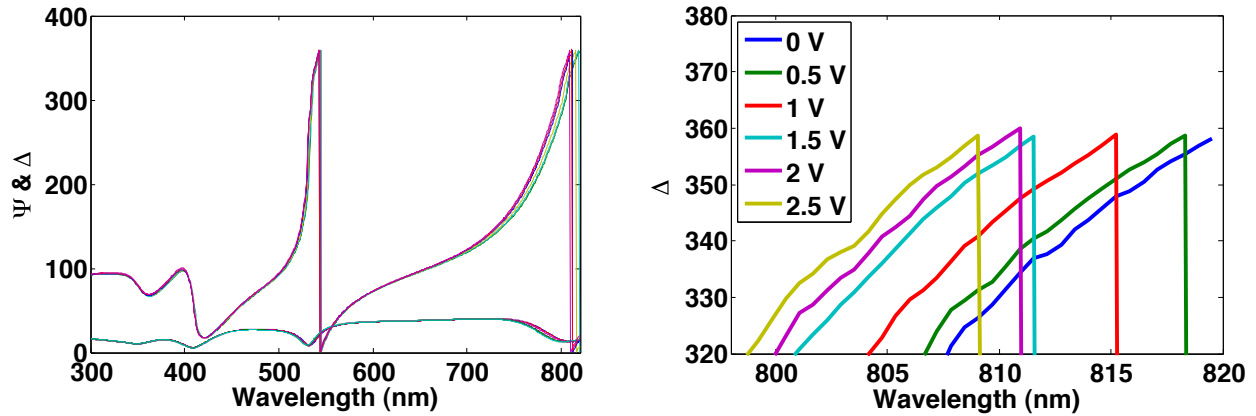## 8.4 Index Shifting in Indium Tin Oxide

Figure 8.3. The ellipsometry measurements of the thin film stack shown in Figure 8.2 from 0 - 2.5 V in 0.5 V steps. The plot on the right focuses on peak shifting around 800 nm.

Ellipsometry measurements of the thin film stack are shown in Figure 8.3 from 0 - 2.5 V in 0.5 V steps. The plot on the left shows both Ψ and Δ over the entire visible spectrum, and the plot on the right is an expanded view of Δ from 795 - 820 nm. The latter plot clearly shows peak shifting with an applied field. Based on the materials parameters determined above, the complex index of refraction for $InTiO_3$ can be calculated using the Drude model. This is shown in Figure 8.4. The complex index of refraction is plotted as a function of wavelength and carrier concentration within the $InTiO_3$ layer from $n = 10^{20} - 10^{22}$ cm^{-3}. Here we see that by changing the carrier concentration within the material by 1 - 2 orders of magnitude, we can shift $\Delta n_{index} \simeq 1$ with negligible Δk.

To determine the change in index of refraction in an $InTiO_3$ accumulation layer, ellipsometry measurements were done on the $Au/InTiO_3/SiO_2/Au$ stack from 0 - 2.5 V in 0.5 V increments. By converting the changes in Ψ and Δ over the visible spectrum, the change in complex index within the accumulation layer was plotted in Figure 8.5. This plot shows that at $\lambda = 500$ nm, $\Delta n_{index} = 0.4$, and at $\lambda = 800$ nm, $\Delta n_{index} = 1.54$! This shift within the ~ 5 nm accumulation layer is a full order of magnitude larger than that seen in traditional electro-optic materials such as lithium niobate [11], and the thickness of this layer was determined using the minimization routine described above. In addition, it can be seen that there is a negligible Δk over the same region. The materials parameters extracted from ellipsometry for each voltage are shown in Table 8.1.
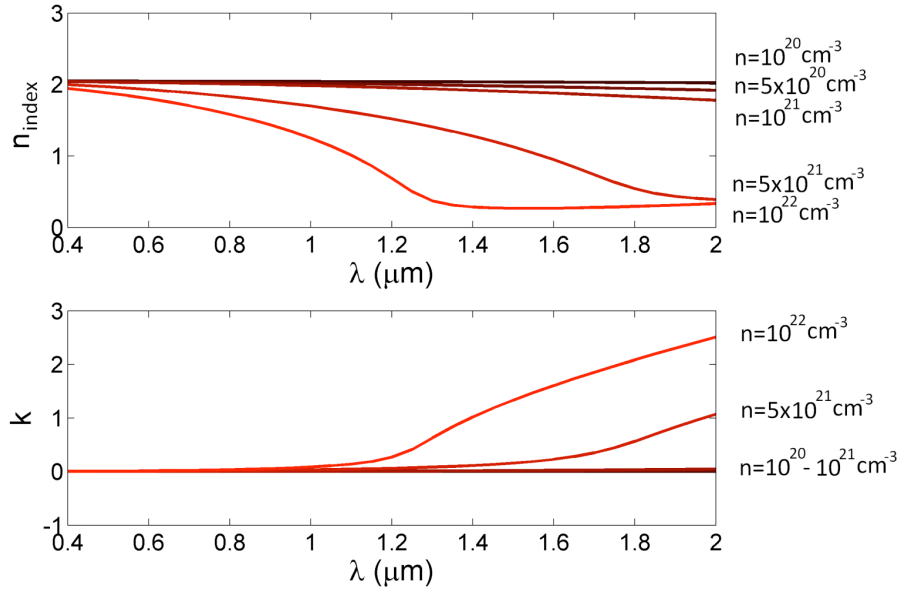
Figure 8.4. Complex index of refraction is plotted as a function of wavelength and carrier concentration within the $InTiO_3$ layer from $n = 10^{20} - 10^{22}$ cm^{-3}.

It should be noted that further studies of the layered structure revealed a number of additional features that indicate a plasma frequency shift from charge accumulation. First, this effect was not observed when a negative voltage was applied to the top, semi-transparent electrode and there was no longer an accumulation layer at the $InTiO_3/SiO_2$ interface. Second, when the thickness of the SiO_2 was doubled, the index shifting was only half as strong for a given voltage, i.e., when the capacitance is reduced. Third, the same amount of peak shifting was observed when the thickness of the $InTiO_3$ layer was increased or decreased, which implies that there was no change in the accumulation layer. Fourth, no peak shifting is observed unless the SiO_2 layer was present. Finally, with similar carrier concentrations, the same effect was also observed in $InZnO_3$. These results all indicate a plasma frequency shift from charge accumulation.

8.5   Mode Modulation in Metal/InTiO$_3$/Metal Waveguides

Based on fitting the ellipsometry data from Figure 8.5, the accumulation layer thickness was determined to be ~ 5 nm. Mode profile modeling was done at $\lambda = 800$ nm for a MIM structure with 50 nm of SiO_2 and $InTiO_3$ between 300 nm of Au. This thickness was chosen so that the metal layers
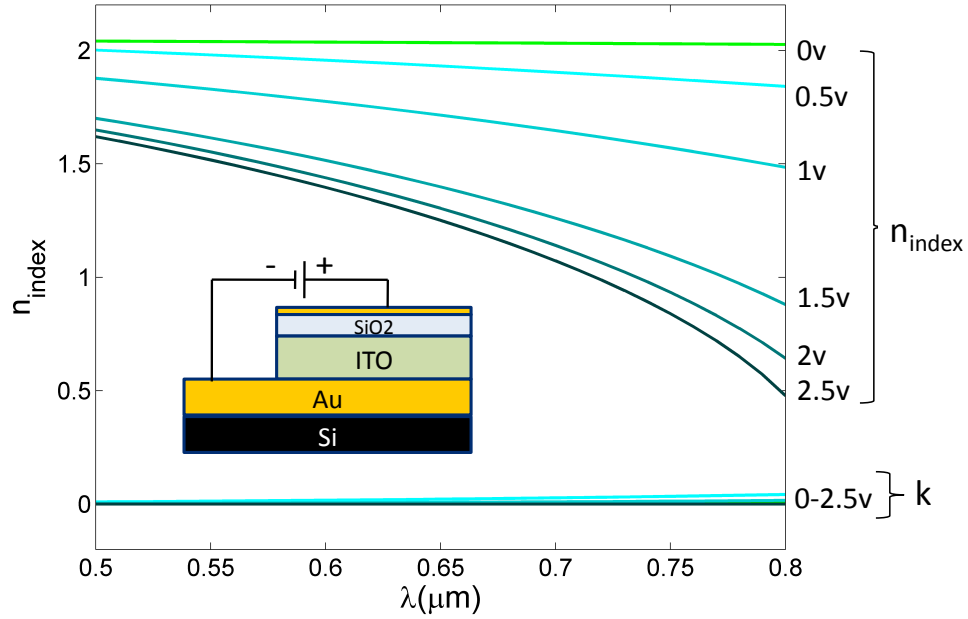
110

Figure 8.5. Complex index of refraction in and InTiO$_3$ accumulation layer as a function of voltage. Both n and k are plotted from V = 0 - 2.5 V.

would be optically opaque. Due to the high modal confinement within this MIM waveguide, driving the InTiO$_3$ into accumulation significantly modulates the plasmon modes within the structure.

Figure 8.6 shows optical mode profiles in the MIM waveguide with (right hand side) and without (left hand side) and applied electric field. The electron distribution across the device under an applied field was calculated by taking the peak concentration of $n_0 = 2.83 \times 10^{22}$ cm^{-3} (Table 8.1) at the InTiO$_3$/SiO$_2$ interface, and plotting the charge distribution base on a solution to Poisson's equation given by:

$$N(x) = n_0 e^{\left(\frac{-x}{L}\right)} \tag{8.4}$$

where "L" is the 5 nm decay length obtained from ellipsometry. n_{index} was calculated for the 20, 1 nm layers next to the InTiO$_3$/SiO$_2$ interface using the Drude model. The mode profile was then calculated and plotted on right hand side of Figure 8.5. With no applied voltage, the mode has an effective index of 2.207. With an applied voltage of 2.5 V, the mode has an effective index of 2.108. This corresponds to a change of $\Delta n_{eff} \simeq 0.1$. In addition, with an applied field a significant portion of the optical mode resides at the SiO$_2$/InTiO$_3$ interface where the accumulation layer is present.

Table 8.1. Parameters used to model the InTiO$_3$ accumulation layer as a function of voltage.

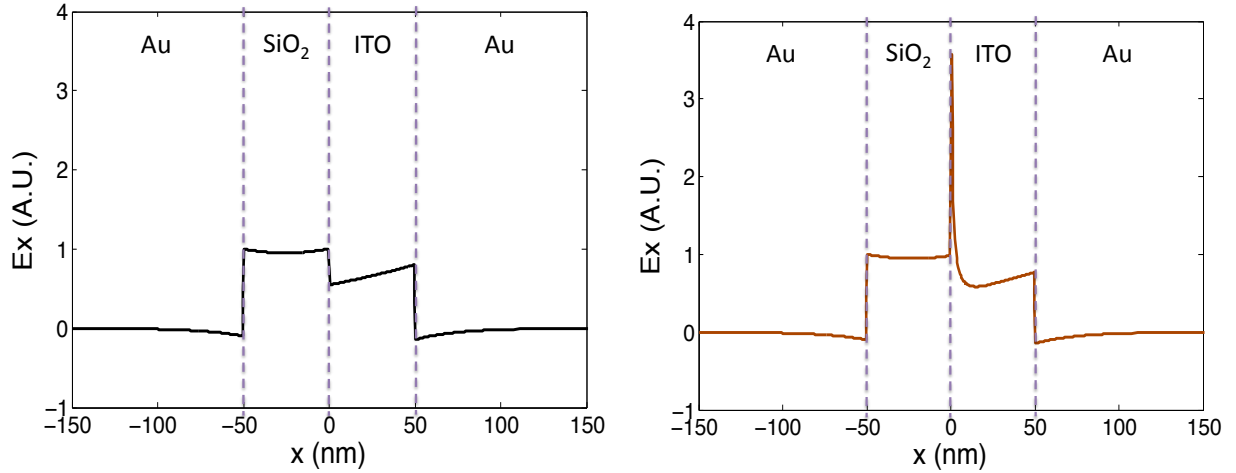| Voltage	ϵ_{inf}	λ_p (nm)	ω_τ (THz)	N (cm^{-3})	$\lambda_p\sqrt{\epsilon_{\text{inf}}}$ (nm)
0	4.21	2310	0.94	1×10^{20}	4.9
0.5	4.41	782	0.36	2.72×10^{21}	1.64
1	4.37	543	0.05	1.65×10^{22}	1.13
1.5	4.25	429	0.00	2.57×10^{22}	0.88
2	4.2	411	0.00	2.77×10^{22}	0.84
2.5	4.16	403	0.00	2.83×10^{22}	0.823

Figure 8.6. Optical Modes in a Au/InTiO$_3$/SiO$_2$/Au Waveguide with (right) and without (left) and applied electric field.

8.6 Conclusion

In this chapter we have shown that TCOs can be used as the active layer in a MIM waveguide, and are useful candidates for active plasmonic devices. We have shown that these materials can be deposited using RF magnetron sputtering and that they can achieve carrier concentrations on the order of 1×10^{19} - 1×10^{21} cm^{-3}. Drude model calculations showed that this placed the plasma frequency at infrared and visible frequencies. Spectroscopic ellipsometry as well as Drude modeling showed that with an applied field these structures can be driven into accumulation and the change in carrier concentration within this accumulation layer can shift the plasma frequency through the visible range of the spectrum. As a result, this produces shifts in the real part of the index of

refraction on the order of $\Delta n = 1$ while maintaining negligible loss within the material. This is a full order of magnitude larger shift that is seen in traditional electro-optic materials such as lithium niobate.

In this part of the thesis, we have shown two types of active plasmonic devices that operates based on modulating the carrier density distribution within a MIM waveguide. These devices have a wide range of flexibility in terms of their operating frequencies and speeds. Since these devices are all majority carrier based, their response time can potentially be even faster than traditional MOS structures. Additionally, their operating frequencies can be tuned across the visible, near, and mid-infrared frequencies by simply changing the device thickness (plasMOStor in Chapter 7) or carrier density (TCOs in Chapter 8). This tunability combined with the fact that silicon and TCOs are already used in an enormous array of applications makes these technologies ideal candidates for integrated optical systems.